NUCL SCI TECH (2019) 30:42
https://doi.org/10.1007/s41365-019-0571-9

High-resolution pixelated CdZnTe detector prototype system for solar hard X-ray imager

Shen Wang[1,2,3] · Jian-Hua Guo[1,2,3] · Yan Zhang[1,2] · Wei Chen[1,2,4]

Received: 6 July 2018 / Revised: 27 August 2018 / Accepted: 1 September 2018 / Published online: 13 February 2019

Abstract A multichannel low-noise electronic prototype system was designed for a pixelated CdZnTe detector. This system is the result of preliminary work on a solar hard X-ray imager, which is one of the three payloads for future solar observations satellite- Advanced Space-based Solar Observatory (ASO-S). A new charge-sensitive amplifier application-specific integrated circuit, VATA450.3, with an on-chip analog-to-digital converter, is used to read out 8×8 anode pixel signals. Two CdZnTe detectors with a thickness of 2 mm and 5 mm were tested. The 2-mm-thick detector achieved energy resolution better than 5% (full-width at half-maximum, FWHM) at 59.5 keV, and the 5-mm-thick detector had better resolution than 1.2% (FWHM) at 662 keV. The design and test results of the prototype system are discussed in this paper.

This work was supported by the National Natural Science Funds of China (Nos. 11622327, 11273070, 11773087, U1631116), the Youth Innovation Promotion Association of the Chinese Academy of Sciences (No. 2014275), and the Strategic Pioneer Program on Space Science of the Chinese Academy of Sciences (No. XDA15010200).

✉ Jian-Hua Guo
jhguo@pmo.ac.cn

[1] Purple Mountain Observatory, Chinese Academy of Sciences, Nanjing 210034, China

[2] Key Laboratory of Dark Matter and Space Astronomy, Chinese Academy of Sciences, Nanjing 210034, China

[3] School of Astronomy and Space Science, University of Science and Technology of China, Nanjing 210034, China

[4] University of Chinese Academy of Science, Beijing 100049, China

Keywords CdZnTe · Readout system · Solar observation · Hard X-ray imager

1 Introduction

Wide bandgap semiconductor cadmium–zinc–telluride (CdZnTe, CZT) can be used in the design of hard X-ray and gamma-ray detectors that are operated at room temperature. The average ionization energy of CdZnTe is much less than that of traditional gas and scintillation detectors. Moreover, CdZnTe detectors have larger average atomic numbers compared to silicon detectors. Therefore, it is possible to achieve superior energy resolution and a high detection efficiency for room-temperature hard X-ray and gamma-ray observations using this detector. In the past two decades, single-polarity charge-sensing techniques have been developed using the small pixel effect [1]. Thus, the poor hole mobility of CdZnTe has been effectively addressed, which has resulted in detectors with excellent performance [2–4]. Pixelated CdZnTe has numerous advantageous properties that are useful in the design of hard X-ray spectroscopy and imaging detectors in astronomy. In recent years, pixelated CdZnTe detectors have been used in many space missions, such as Swift [5], NuSTAR [6] and EXIST [7].

Advanced Space-based Solar Observatory (ASO-S) [8] is the first Chinese satellite mission dedicated to solar physics research. The mission aims to explore the connections between solar magnetic field, solar flares, and coronal mass ejections (CMEs). The satellite has three payloads onboard: the full-disk solar vector magnetograph, the Lyman-alpha Solar Telescope, and the solar hard X-ray imager (HXI). The HXI will be used to image the full solar

disk in the energy range of 30–300 keV using indirect imaging techniques via spatial modulation. During the prototype stage, a readout system with CdZnTe detectors is a feasible solution for solar hard X-ray indirect imaging.

In this paper, we report on the electronics design and experimental results of a multipixel CdZnTe detector prototype system, which could be used as a substitute for HXI in the future. A brief introduction to the HXI is presented in Sect. 2. Then we describe the design methods for CdZnTe detectors prototype in Sect. 3, which includes the hardware arrangement and software development. We have evaluated the system's root mean square (RMS) noise and linearity performance. In addition, different CdZnTe detectors were tested using ^{241}Am and ^{137}Cs radioactive sources. The results and discussion of this process is presented in Sect. 4. A summary of the main conclusions is presented in Sect. 5.

2 Hard X-ray imager (HXI)

The HXI mainly consists of a collimator, a calorimeter, and an electrical control box, as shown in Fig. 1. The collimator modulates the intensity of the hard X-ray and measures the positional deviation between the optical axis and the center of the sun. The calorimeter measures the energy of the X-ray photons that are modulated by the collimator, the counts of photons that are incident during different operational situations, and accumulates an energy spectrum according to preinstalled parameters. The electronic box supplies power to the collimator and calorimeter and also manages scientific data reception and remote data transmission (Table 1).

The calorimeter contains detectors, high-voltage (HV) supplies, and the readout electronics. We plan to use CdZnTe semiconductor detectors for hard X-ray measurement and counting. When hard X-ray photons are incident on the CdZnTe detectors, charge signals are measured by a charge-sensitive amplifier chip placed in the front-end electronics board. According to the relevant operating parameters, time and energy information is accumulated in a given time interval. Case-by-case recording and sub-threshold counting are also performed. The scientific data are compiled together with current, temperature, and other engineering parameters and sent to the electronic control box. The HV fan-out board provides independent bias voltages to the CdZnTe detectors to ensure that even if a short-circuit fault occurs, the HV to other detectors is still within the operating range of the HV power module.

Table 1 Summary of the design parameters and expected performance of HXI

Parameter	Value
Effective area (cm^2)	200
Energy range (keV)	$30 - 200$
Energy resolution	$\leqslant 27\%$ @ 33keV
Temporal resolution (s)	$\leqslant 0.5$
Angular resolution	$\leqslant 6''$ @ 3keV
Field of view (FoV)	$> 32'$

3 Prototype system

3.1 Overview

During the research and development stage of the satellite project, we designed a readout electronic prototype for the pixelated CdZnTe detectors. Figure 2 represents a scheme that contains the main signal sets and the schematic list for this system. The system can be divided into a hybrid board and a data acquisition (DAQ) board. The hybrid board has one multipixel CdZnTe detector and one integrated charge-sensitive amplifier chip VATA450.3. The detector and hybrid printed circuit board (PCB) are joined together using Samtec high-density connectors. Die

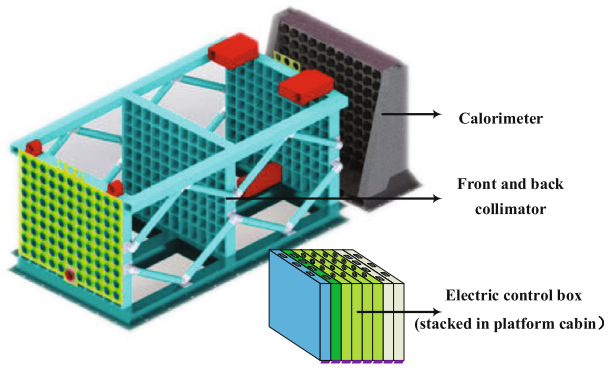

Fig. 1 (Color online) Schematic view of the HXI detector

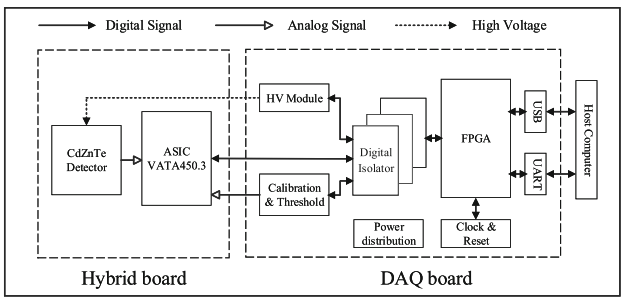

Fig. 2 Block diagram of the CdZnTe detector prototype system

application-specific integrated circuit (ASIC) was wire-bonded onto the hybrid board to reduce input noise.

The DAQ board is responsible for receiving commands from the host computer, controlling the work mode of the hybrid board, in addition to packing and uploading digital data to the host computer. The core of this board is an Intel field-programmable gate array (FPGA) clocked with an external 20 MHz crystal oscillator. The FPGA reads commands from the host and configures ASIC for different working modes, provides an event first-in-first-out for data buffering and packing, and controls the high-voltage module by supplying a bias voltage of up to −1250 V to the CdZnTe detectors in the hybrid board. The DAQ board provides calibration pulses and threshold voltages for VATA450.3. Communication with the host computer occurs via universal serial bus and the universal asynchronous receiver/transmitter interface.

When a hard X-ray or gamma-ray photon is incident on the CdZnTe detector, a large number of electron–hole pairs proportional to the deposited energy are generated. Under the application of a high electric field, the electrons and holes drift toward the anode and cathode, respectively. To improve energy resolution, we primarily selected electronic signals induced on the anode pixels according to single-polarity charge-sensing techniques. The VATA450.3 chip collects the analog electronic signals and converts them into digital bits before sending them to the FPGA. The digital data are then uploaded to the host computer for real-time analysis or offline processing.

3.2 Pixelated CdZnTe detectors

CdZnTe crystals are considered as one of the most promising compound semiconductors for application in space mission X-ray and gamma-ray detection. Crystal growth is the primary step that affects material properties and consequently detector performance. Most commercial detector-grade CdZnTe crystals are produced by eV Products in the USA, Redlen Technologies in Canada, and Orbotech Company in Israel at very high prices. In the 1990s, some Chinese institutions began developing CdZnTe crystals growing techniques. For example, Zha et al. of Northwestern Polytechnical University have grown CdZnTe crystals with single-crystal diameters of more than 60 mm, bulk resistivity up to 4×10^{10} Ω, and $\mu\tau$ over 2×10^{-3} cm^2/V [9].

We used CdZnTe crystals manufactured by Imdetek Company. Two types of detectors are shown in Fig. 3, and the main parameters are summarized in Table 2. Both detectors consist of 8×8 pixels, and each pixel is 1.1 mm × 1.1mm. One dimension of the hard X-ray detection is 10 mm × 10 mm × 2mm, and the other is 10 mm × 10 mm × 5 mm for the soft gamma-ray detection. The magnitude of the applied electric field of the detectors is approximately 200 volts per millimeter. The current width of the detectors which is dependent on the bias voltage and the absorption position of the detector is approximately 200 nanoseconds when incident X-rays strike a pixel. All 64 pixels are read out by one ASIC.

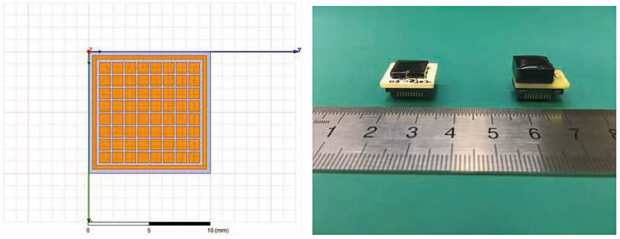

Fig. 3 (Color online) (Left) Anode pixel pattern of CdZnTe detectors with guard-ring. (Right) 2-mm and 5-mm-thick detectors. Samtec high-density connectors are positioned under the CdZnTe pixel detectors

Table 2 Parameters of CdZnTe pixel detectors

Parameter	Value	
Material	CdZnTe	
Density (g/cm^3)	5.78	
Resistivity (Ωcm)	$> 10^{10}$	
Pixel size (mm^2)	1.1×1.1	
Pixel array	8×8	
Electrode material	Au	
Working temperature (°C)	−20 to +40	
Detector thickness (mm)	2.0 ± 0.1	5.0 ± 0.2
Energy range (keV)	6–350	20–700

3.3 VATA450.3

Space missions have strict requirements for the volume of satellite payloads. In addition, high-precision X-ray imaging requires low-noise front-end electronics. It is difficult for traditional discrete circuits to meet these requirements. Recently, charge-sensitive amplifier ASICs have been widely used in space projects because of their small size and low noise. Chip VATA450.3 produced by Norway IDEAS was utilized in this electronic prototype system, and it was applied in the hybrid board to collect the charge signals generated by the CdZnTe detector.

The three main components are included in this chip, as shown in Fig. 4, and include the Viking amplifier (VA), trigger amplifier (TA), and on-chip analog-to-digital converter (ADC). One VATA450.3 chip has 64 identical channels. In the VA component, each channel has a

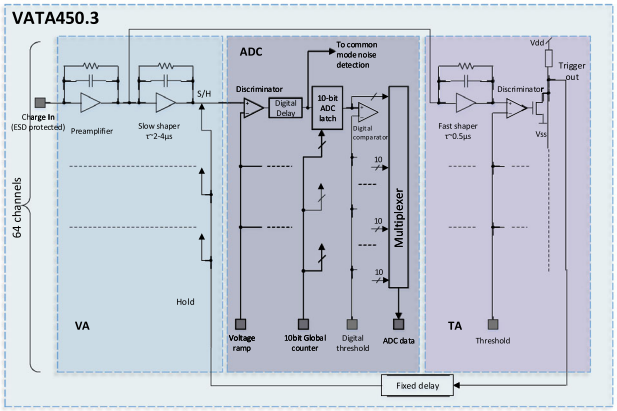

Fig. 4 (Color online) Functional structure of VATA450.3 ASIC

preamplifier, a slow shaping amplifier, and a peak-hold and sample-hold circuit. For the anode pixels connected directly to the ASIC input pads (DC coupled), a leakage current compensation circuit is added to each channel. In the TA component, each channel has a fast shaper and a discriminator for triggering. A trigger mask can be set to disable channels with high noise. In the ADC component, each channel has a voltage comparator, a Wilkinson-type ADC with 10 bits latch, a digital comparator and a multiplexer. All amplifier inputs are protected against overvoltage and electrostatic discharge. The main parameters are summarized in Table 3. For example, this chip has two kinds of dynamic range for operation under different gain modes. The max input charge can be ±40 fC. The pair creation energy of CdZnTe is approximately 4.64 eV. Therefore, this chip can measure gamma-ray energies up to 1 MeV.

3.4 FPGA logic

FPGAs are widely used due in part to their large number of input/output pins and ease of debugging. Among them, Cyclone series FPGAs are cost-effective and can realize logic control and DAQ functions of the DAQ board in this electronic system. The DAQ board used an Intel FPGA (Cyclone-III EP3C16Q240C7). We designed an FPGA control logic using Verilog hardware description language.

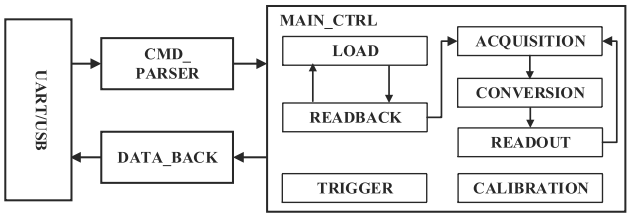

Fig. 5 FPGA logic diagram

The function blocks of logic are shown in Fig. 5. Our logic was divided into different function modules for ease of use and updating.

3.5 Host software

Based on LabWindows/CVI, we developed a host control software for the prototype system. LabWindows/CVI is an interactive C language operating platform supported by National Instruments (NI), which is widely used in system inspection, industrial control, and DAQ. Figure 6 shows the user interface that can realize functions including the generation and storage of commands, offline data storage and analysis, and status monitoring of the chip.

4 Results and discussion

4.1 Linearity and RMS noise

Firstly, we tested the linearity properties of the readout electronics system without the CdZnTe detector. Because the VATA450.3 chip has an internal test pulse generator, it is possible to calibrate this chip without the need for an external circuit or a signal generator. When this chip is operated in calibration mode, different step test pulses are generated based on the chip's configuration register. After those step pulses are injecting into the chip, it is possible to measure the chip's linearity responses. Some test results are presented in Fig. 7. VATA450.3 has four kinds of input charge ranges including 0 to 16 fC, 0 to −16 fC, 0 to 40 fC, and 0 to −40 fC. The average integral nonlinearity (INL) of these four ranges is 1.83%, 2.26%, 1.90%, and 0.74%.

Table 3 Summary of the design parameters and expected performance of HXI

Parameter	Value
Supplier	IDEAS
Technology	0.35 μm CMOS
Chip size	10,000 μm × 6500 μm × 450 μm ($L \times W \times H$)
Dynamic range	±16 fC, ±40 fC
Readout rate	10MHz (Max.)
Power consumption	255 μW/channel(default setting)
ENC	$59e^-$ (default mode, no inputs bonded)

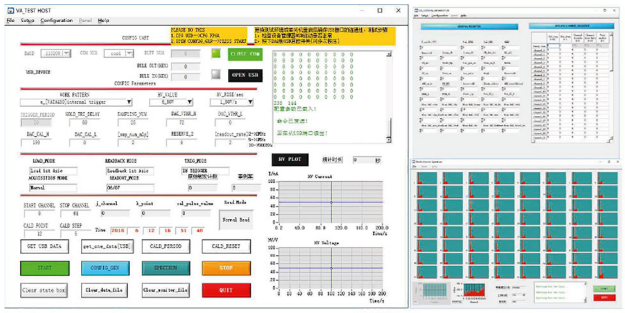

Fig. 6 (Color online) User interface of the host program

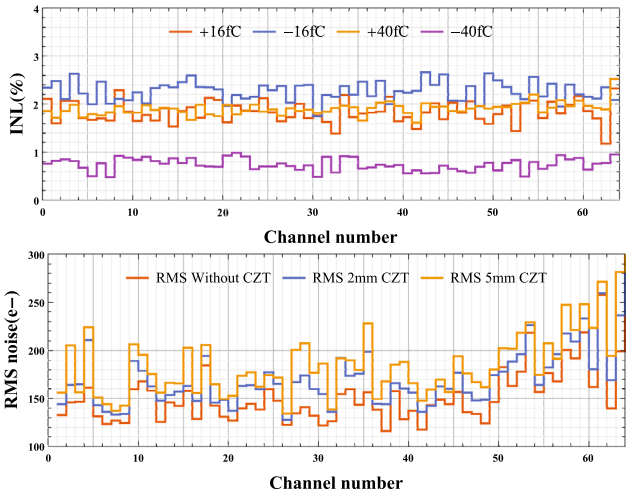

Fig. 7 (Color online) System linearity and RMS noise performance. The top plot shows the INL of the four input range modes. The bottom plot is the RMS noise performance under different conditions

Almost all channels exhibit good linearity and consistency, while the chip's last channel has a higher pedestal.

The noise level of the charge-sensitive preamplifier has a linear relationship with the input load capacitance. The equivalent noise charge (ENC) is often used to represent the noise level of electronics readout systems. The relationship between the preamplifier ENC and its load capacitance can be expressed as [10]:

$$\mathrm{ENC_{preamp}} = \frac{1}{\sqrt{t_\mathrm{p}}}(K_1 + K_2 C_\mathrm{t}), \tag{1}$$

where Ct is the total load capacitance at the input of the channel, tp is the shaping time of the VATA450.3 chip, and K_1 and K_2 are considered to be constant during operation. In this prototype system, the input PCB wire and CdZnTe detector are major contributors to the input load capacitance. We tested the system's RMS performance under different load capacitance values. If detectors were not installed, the average noise of the 64 channels was 154e$^-$. With the 2-mm-thick and 5-mm-thick CdZnTe detectors assembled in the front hybrid board, the noise levels are 172e$^-$ and 186e$^-$, respectively. Obviously, the system noise will be higher for larger input capacitance values. The ENC performance is shown in Fig. 7 bottom plot.

4.2 Spectral performance

After some functional tests, we performed radiation source testing of the CdZnTe detector prototype system. Initially, we set an appropriate trigger threshold to discriminate between signals. When X-rays or gamma-ray photons are incident on the CdZnTe detector, the deposited charge is collected by one of the chip's 64 channels. The ASIC processes the charge signal above the threshold into binary data. These data are then packed and uploaded to the host. One trigger-event data frame has 731 bits. These bits contain 64 channel ADC values, the common-mode data, and reference data of the dummy channel. Each original pixel ADC value for one event has multiple components [11]:

$$\mathrm{ADC}_{ij} = \mathrm{Ped}_i + \mathrm{CN}_j + \mathrm{Noise}_{ij} + \mathrm{Signal}_{ij}, \tag{2}$$

ADC_{ij} is the ith channel ADC value for the jth event, Ped_i is the pedestal value of channel i, and CN_j is the common noise value. The common noise of each channel is identical for a given sample. Noise_{ij} represents random noise and $Signal_{ij}$ is the true value of each channel for an event. After source testing, we performed pedestal deduction and common-mode noise correction on the origin data. In the future, we will design a collimation platform for charge-sharing research.

The 64-pixel 2mm-thick guard-ring CdZnTe detector was biased at −500 V and maintained at room temperature. A 19-mCi ^{241}Am source was arranged to test the spectrum performance of the prototype system. During the testing, it was determined that the last ASIC channel generates significant noise in chip internal trigger mode; therefore, we disabled the last channel (channel 64). The spectral results are shown in Fig. 8. Apart from the last channel, all channels show good spectrum performance. The average full-width at half-maximum (FWHM) at the 59.5 keV peak is 5.45% with a resolution down to 4.99%.

We also tested a 5-mm-thick guard-ring CdZnTe detector biased at −1000 V using a ^{137}Cs source. When the 662 keV gamma-ray was incident on the CdZnTe detector, most of the events are Compton scattering events and the photoelectric effect cross section is very low. All 64-channel data are merged together to obtain the spectrum which is shown in Fig. 9. The FWHM at 662 keV is approximately 1.18%.

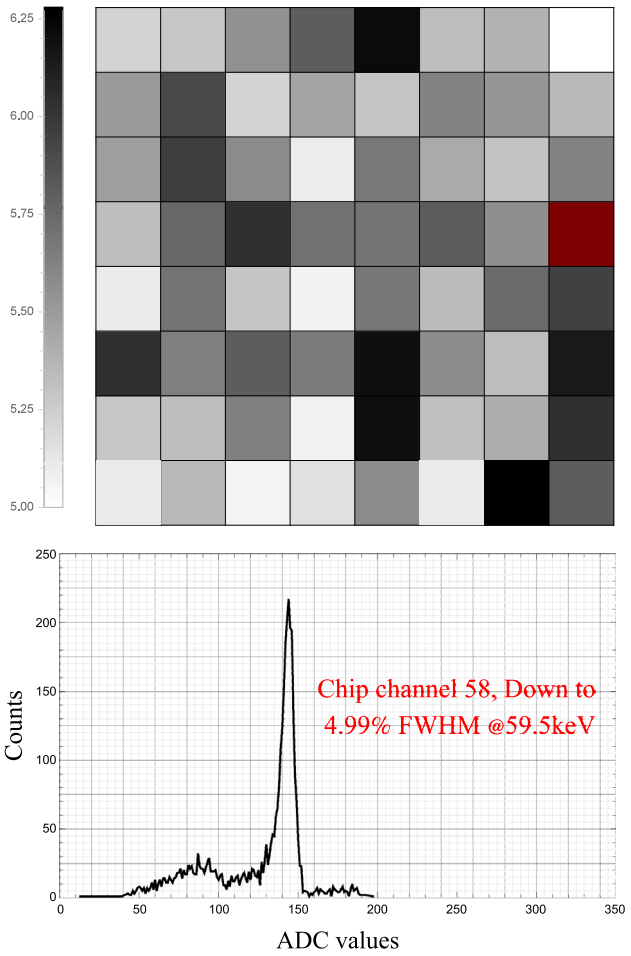

Fig. 8 Prototype performance of 2-mm-thick CdZnTe when testing with ^{241}Am resource. (Top) Gray plot shows FWHM (%) of all 64 pixels. The white grids represent the lower FWHM, while the black grids represent the higher FWHM. The red grid represents dead pixels that are connected to the 64th channel. (Bottom) ^{241}Am spectrum of the 58th channel

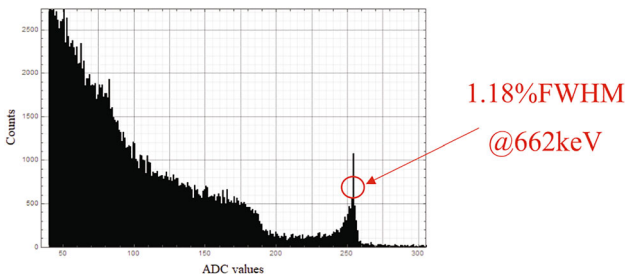

Fig. 9 5-mm-thick CdZnTe detector spectral results using 3 μCi Cs137 source

5 Conclusion

We successfully designed a low-noise readout electronic system for a 64-pixel CdZnTe detector. This system is suitable for a wide input photon range from 10 to 1000 keV. The overall ENC of the prototype system was approximately 200e$^-$. The spectral results show that this electronic system adequately meets the requirements of the HXI prototype stage for solar hard X-ray observations. In a future study, we plan to perform studies on the charge-sharing effect and the photon depth of interaction in a CdZnTe detector to optimize energy resolution.

References

1. H.H. Barrett, J.D. Eskin, H.B. Barber, Charge transport in arrays of semiconductor gamma-ray detectors. Phy. Rev. Lett. **75**, 156 (1995). https://doi.org/10.1103/PhysRevLett.75.156
2. F. Zhang, Z. He, G.F. Knoll et al., 3-D position sensitive CdZnTe spectrometer performance using third generation VAS/TAT readout electronics. IEEE. T. Nucl. Sci. **52–5**, 2009 (2005). https://doi.org/10.1109/TNS.2005.856821
3. A. Brambilla, P. Ouvrier-Buffet, G. Gonon et al., Fast CdTe and CdZnTe semiconductor detector arrays for spectroscopic X-ray imaging. IEEE. T. Nucl. Sci. **60–1**, 408 (2013). https://doi.org/10.1109/TNS.2012.2226910
4. K. Lee, J.W. Martin, A. Garson et al., Development of CZT detectors for X-ray and gamma-ray astronomy. Proc. SPIE **8142**, 81420D (2011). https://doi.org/10.1117/12.893595
5. N. Gehrels, G. Chincarini, P. Giommi et al., The Swift gamma-ray burst mission. APJ **611**, 1005 (2004). https://doi.org/10.1086/422091
6. F.A. Harrison, W.W. Craig, F.E. Christensen et al., The nuclear spectroscopic telescope array (NuSTAR) high-energy X-ray mission. APJ **770**, 103 (2013). https://doi.org/10.1088/0004-637X/770/2/103
7. J. Grindlay, N. Gehrels, F. Harrison et al., EXIST's gamma-ray burst sensitivity. Proc. AIP **662**, 477 (2003). https://doi.org/10.1063/1.1579406
8. W.Q. Gan, Y.Y. Deng, H. Li et al., ASO-S: Advanced Space-based Solar Observatory. Proc. SPIE **9604**, 96040T (2015). https://doi.org/10.1117/12.2189062
9. G.Q. Zha, T. Wang, Y.D. Xu et al., The development of CZT semiconductor X-ray and g-ray detectors. Physics **12**, 007 (2013). https://doi.org/10.7693/wl20131205
10. O. Toker, S. Masciocchi, E. Nygård et al., VIKING, a CMOS low noise monolithic 128 channel frontend for Si-strip detector readout. Nucl. Instrum. Methods Phys. Res. Sect. A **340–3**, 572 (1994). https://doi.org/10.1016/0168-9002(94)
11. Y.F. Dong, F. Zhang, R. Qiao et al., DAMPE silicon tracker on-board data compression algorithm. Chin. Phys. C **39–11**, 116202 (2015). https://doi.org/10.1088/1674-1137/39/11/116202